Equation Chapter 1 Section 1AIMETA 2019
Equation Chapter 1 Section 1XXIV Conference
The Italian Association of Theoretical and Applied Mechanics
Rome, Italy, 15-19 September 2019

SHAKE TABLE TESTING OF A TUNED MASS DAMPER INERTER (TMDI)-EQUIPPED STRUCTURE AND NONLINEAR DYNAMIC MODELING UNDER HARMONIC EXCITATIONS

Daniele Pietrosanti[1], **Maurizio De Angelis**[1] **and Agathoklis Giaralis**[2]

[1] Department of Structural and Geotechnical Engineering, Sapienza University of Rome
Via Eudossiana 18, 00184, Rome, Italy
e-mail: daniele.pietrosanti@uniroma1.it; maurizio.deangelis@uniroma1.it

[2] Department of Civil Engineering, City, University of London
Northampton Square, EC1V 0HB, London, United Kingdom
e-mail: agathoklis.giaralis.1@city.ac.uk

Keywords: Inerter, tuned mass damper inerter, shaking table testing, nonlinear dynamic model, high damping rubber bearings.

Abstract. *This paper presents preliminary experimental results from a novel shaking table testing campaign investigating the dynamic response of a two-degree-of-freedom (2DOF) physical specimen with a grounded inerter under harmonic base excitation and contributes a nonlinear dynamic model capturing the behavior of the test specimen. The latter consists of a primary mass connected to the ground through a high damping rubber isolator (HDRI) and a secondary mass connected to the primary mass through a second HDRI. Further, a flywheel-based rack-and-pinion inerter prototype device is used to connect the secondary mass to the ground. The resulting specimen resembles the tuned mass damper inerter (TMDI) configuration with grounded inerter analytically defined and numerically assessed by the authors in a number of previous publications. Physical specimens with three different inerter coefficients are tested on the shake table under sine-sweep excitation with three different amplitudes. Experimental frequency response functions (FRFs) are derived manifesting a softening nonlinear behavior of the specimens and enhanced vibration suppression with increased inerter coefficient. Further, a 2DOF parametric nonlinear model of the specimen is established accounting for non-ideal inerter device behavior and its potential to characterize experimental response time-histories, FRFs, and force-displacement relationships of the HDRIs and of the inerter is verified.*

1 INTRODUCTION

Passive vibration suppression in dynamically excited building structures is commonly implemented through one, or a combination, of the following three types of devices: dampers, vibration isolators, and dynamic vibration absorbers or tuned mass dampers (TMDs). In recent years, inerter-based passive vibration suppression configurations emerged, the most widely considered being the tuned viscous mass damper (TVMD) [1], the tuned inerter damper (TID) [2] and the tuned mass damper inerter (TMDI) [3, 4], by coupling dampers and TMDs with an *inerter*. The latter is a device developing acceleration-dependent force proportional to a constant termed *inertance* and assuming mass units [5]. Through pertinent numerical work, it was established that these configurations achieve secondary attached mass reduction and/or improved vibration control efficiency in fixed-based (e.g., [6-7]) as well as in base isolated building structures (e.g., [8, 9]). Moreover, Basili et al. [10, 11] demonstrated the effectiveness of linking adjacent building structures through inerter-based connections to improve their performance to dynamic loads.

All the above theoretical studies adopted linear structural models and assumed that the inerter behaves as an ideal linear mass-less mechanical element with arbitrarily high inertance as defined by [5]. Nevertheless, prototyped inerter devices deviate from the ideal inerter behavior due to various effects dependent on the specifications, operational frequency range, and technology used to implement the inerter (i.e., mechanical, hydraulic, or fluid-base inerters). In this regard, lately, the influence of non-ideal inerter behavior to the vibration suppression potential of various inerter-based configurations has been quantified either numerically, by representing inerter elements using nonlinear force-deformation relationships fitted into experimental data (e.g., [12, 13]), or experimentally (e.g., [14, 15]). Still, research work accounting for non-ideal inerter behaviour has thus far exclusively considered linear structural behaviour whereas in several applications, notwithstanding earthquake engineering, structures as well as absorbers may behave in a nonlinear fashion.

To this end, this paper contributes a first study examining experimentally, through shaking table testing, the behavior of a TMDI with a grounded non-ideal inerter device, attached to a base-excited single-degree-of-freedom (SDOF) structure in which the structure as well as the TMDI behave nonlinearly. A nonlinear numerical model of the physical specimen is also developed and its capacity to capture the response of the physical model is verified by comparison with experimental data. The remainder of the paper is organized as follows: Section 2 describes the physical model, shaking table setup, and instrumentation used in the experimental testing; Section 3 reports and discusses frequency response functions from experimental data; Section 4 fits experimental data to an appropriately defined parametric nonlinear model characterizing the nonlinear structural response behaviour; Section 5 summarizes concluding remarks.

2 PHYSICAL MODEL, SHAKING TABLE SETUP, AND INSTRUMENTATION

A custom-built test specimen (physical model) is used throughout this paper approximating the lumped-mass two-degree-of-freedom (2DOF) numerical model of a TMDI-equipped SDOF structure with grounded inerter defined in [3, 4]. An annotated photo of the specimen mounted on the uni-axial shake table in the Materials Testing Laboratory at Sapienza, University of Rome, is shown in Figure 1 together with a cross-section along the excitation axis. The specimen comprises: (i) a SDOF primary structure (PS) consisting of the primary mass, m_I=125kg, materialized by two mild steel plates (78cm×68cm×1.5cm) bolted together and connected to the ground (shake table) through a primary high damping rubber isolator (HDRI), (ii) a TMD consisting of the secondary mass, m_T= 10kg (i.e., mass ratio $\mu=m_T/m_I$ 8%), materialized by a

80cm long steel beam with hollow rectangular cross-section (10cm×5cm and 3mm wall thickness), connected to the PS (primary mass) through a secondary HDRI, and (iii) an in-house built inerter device connecting the TMD (secondary mass) to the ground/shake table. Both HDRIs are cylindrical with specifications: 58mm of diameter, 80mm of height, and 54mm total rubber thickness (27 rubber layers of 2mm thickness each). The inerter device uses a rack-and-pinion mechanism to drive a flywheel through an off-the-shelf gearbox [4]. Three different nominal inertance values, b, or inertance ratios, $\beta=b/m_I$, are considered: β_1=0.1% (negligible inertance with no flywheel, NF case); β_2=38.3% or b_2=47.9kg (intermediate inertance with one spur gear flywheel, IF case, shown in Figure 1); β_3=76.5% or b_3=95.6kg (large inertance with two spur gears flywheel, LF case). Further details on the specifications and the assembly of the inerter device are found in Pietrosanti [16].

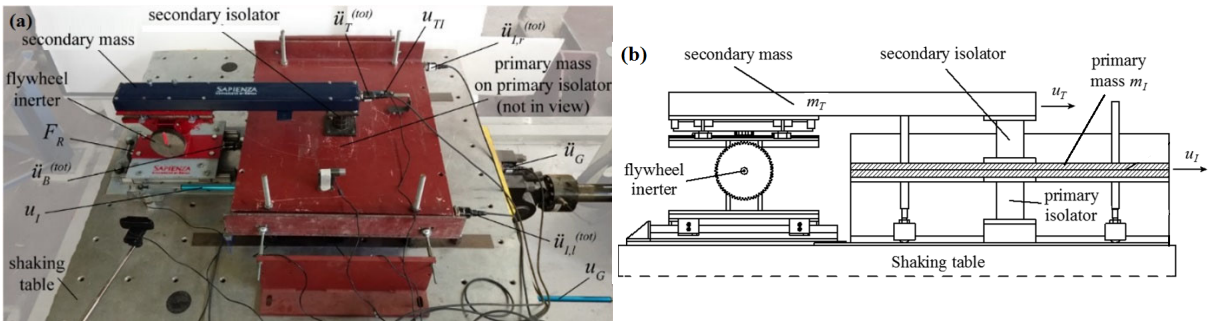

Figure 1: (a) Photo of the experimental setup and arrangement of instrumentation, (b) Longitudinal cross-section of the physical TMDI-equipped SDOF model with grounded flywheel-based inerter.

The experimental setup used to test the physical model is instrumented with 5 piezoelectric accelerometers indicated in Figure 1(a) as follows: one placed on the shake table measuring input horizontal (ground) acceleration, $\ddot{u}_G$; two placed at the two ends of the primary mass plate measuring total horizontal acceleration, $\ddot{u}_{I,r}^{(tot)}$ and $\ddot{u}_{I,l}^{(tot)}$, from which total primary mass response acceleration is obtained as $\ddot{u}_I^{(tot)} = (\ddot{u}_{I,l}^{(tot)} + \ddot{u}_{I,r}^{(tot)})/2$; one placed on the secondary mass beam measuring total horizontal acceleration $\ddot{u}_T^{(tot)}$; and one placed at the inerter support measuring total horizontal acceleration $\ddot{u}_B^{(tot)}$. From the last two accelerometers, the relative acceleration of the secondary mass is obtained as $\ddot{u}_T = \ddot{u}_T^{(tot)} - \ddot{u}_B^{(tot)}$. Further, three displacement sensors are used measuring relative displacement between (a) the shake table and the lab floor (fixed reference point), u_G, (b) the primary mass and the shake table mass, u_I, and (c) the secondary mass and the primary mass, $u_{TI} = u_T - u_I$. From the last two measurements, the deflection of the primary structure is obtained as $u_T = u_I + u_{TI}$. Finally, a load cell is used to measure the force transmitted by the inerter to the shaking table, F_R. Using this load cell measurement, it is possible to obtain the inerter device force as $F_B = F_R + m_B\ddot{u}_B^{(tot)}$, where m_B is the mass of the inerter device and its support equal to 16.7kg for NF case, 18.8kg for IF case, and 20.9kg for LF case. Then, the resisting forces at the primary and the secondary HDRIs can be retrieved as $F_T = -F_B - m_T\ddot{u}_T^{(tot)}$ and $F_I = F_T - m_I\ddot{u}_I^{(tot)}$, respectively.

3 FREQUENCY DOMAIN EXPERIMENTAL RESPONSE CHARACTERIZATION

The above physical TMDI-equipped SDOF models are subject to a set of constant amplitude sine-sweep shake table excitations with increasing and decreasing stepped frequency changes at 0.05Hz near system resonant frequencies and at 0.1Hz away from resonant frequencies within the range [1Hz 10Hz]. At each step, 20 full excitation cycles are considered to reach

steady-state response conditions. Appropriate displacement-controlled excitation signals are used to achieve three different peak ground acceleration values: PGA=0.05g, 0.10g and 0.15g.

Typical selective total response acceleration time-histories of the primary mass are plotted in Figure 2 for sine-sweep excitation with PGA=0.10g amplitude. For the uncontrolled PS (no TMDI attached), it is seen that response time-histories for sine-sweep excitation with increasing and decreasing frequency do not overlap while the peak response (i.e., dynamic amplification) is higher and occurs earlier for the sine-sweep with decreasing frequency demonstrating a softening nonlinear behavior of the primary HDRI (Figure 2(a)). However, the TMDI-equipped PS responds in an almost linear fashion attaining reduced peak amplitude by about 50% compared to the uncontrolled PS. The response of the latter 2DOF structure attains two local peaks at different time instants corresponding to two resonant frequencies (Figure 2(b)), while its first local peak occurs earlier in time than the (single) local peak of the PS in Figure 2(a) indicating a shift of the PS resonant frequency to lower frequencies due to the attached TMDI.

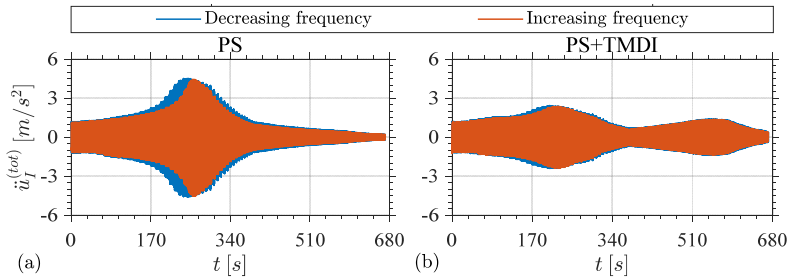

Figure 2: Time histories of PS acceleration, $\ddot{u}_I^{(tot)}$, under sine-sweep excitation with increasing and decreasing frequency for: (a) uncontrolled PS and (b) PS+TMDI ($\beta_2 = 0.383$, $PGA = 0.10g$).

The nonlinear behavior of the physical model and its resonant frequencies are further traced in the frequency domain in Figure 3 plotting experimental PS displacement and acceleration frequency response functions (FRFs) for different excitation amplitudes (PGA) and inertance ratios (β) normalized by the excitation FRF. It is seen that resonant structural frequencies reduce as the excitation amplitude (PGA) increases (location of peak FRF values shift to the left) confirming an overall softening nonlinear system behavior. It is further seen that TMDI effectiveness in suppressing PS deflection increases with increasing inertance, though this is not necessarily true for PS response acceleration to broadband or to high frequency (above 4Hz) narrowband excitations which confirm analytical results reported in [9].

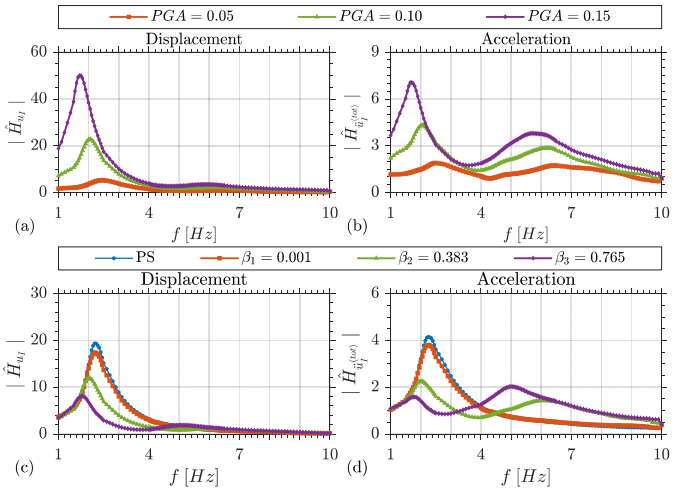

Figure 3: Normalized FRFs of displacement and acceleration of PS for various: (a-b) amplitudes for TMDI controlled PS with fixed β_2=38.3%; and (c-d) inertance ratios for fixed PGA=0.10g.

4 NONLINEAR NUMERICAL MODELING AND ASSESSMENT

A nonlinear parametric 2DOF numerical model is developed to capture the response of the physical model in Figure 2 under shaking table excitations examined in previous sections. The DOFs of the model correspond to lateral deflections of the primary and secondary masses, u_I and u_T, respectively, as shown in Figure 4(a). A linear dashpot in parallel with a nonlinear elastic spring, observing a parametric polynomial expression (see e.g., [17]), are used to represent the two HDRIs as per the following force-deformation relationships

$$\begin{aligned} F_{EI} &= k_{1I}u_I - k_{2I}u_I^2 sign(u_I) + k_{3I}u_I^3, \;\; F_{DI} = c_I\dot{u}_I \\ F_{ET} &= k_{1T}u_{TI} - k_{2T}u_{TI}^2 sign(u_{TI}) + k_{3T}u_{TI}^3, \;\; F_{DT} = c_T(\dot{u}_T - \dot{u}_I) \end{aligned} \tag{1}$$

where F_{EI} and F_{DI} are the resisting forces of the nonlinear spring and the dashpot, respectively, of the primary HDRI, and $F_{E\,T}$ and F_{DT} are the corresponding forces of the secondary HDRI. In the last expressions, k_{jI} and k_{jT} (j=1,2,3) are coefficients characterising the behaviour of the primary and secondary nonlinear spring, respectively, while c_I and c_T are the damping coefficients for the primary and secondary isolators, respectively. Further, a dot over a symbol denotes time differentiation and $sign(x) = 1$ for $x > 0$ and $sign(x) = -1$ for $x < 0$.

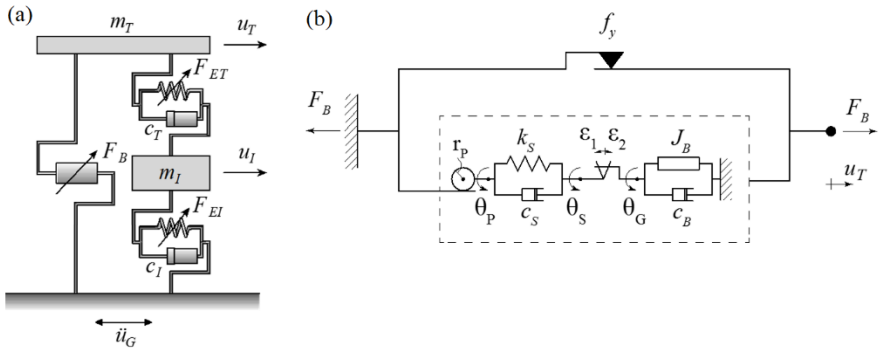

Figure 4: (a) Nonlinear 2-DOF numerical model characterizing the physical system of Figure 1 (an arrow above an element indicates nonlinear element behaviour), (b) Nonlinear mechanical model of the rack-and-pinion flywheel-based inerter included in the physical model.

Moreover, the inerter device is represented by the mechanical model in Figure 4(b) discussed in detail by [16], where r_P is the radius of the pinion transforming the translational into rotational motion, J_B is the flywheel moment of inertia, f_y, is the coefficient of the coulomb friction element accounting for friction effects of the rack-and-pinion device mechanism, c_B is the dashpot damping coefficient accounting for parasitic damping in the device, and ε_1 and ε_2 are the clearances of the double-sided backlash gap element accounting for the so-called "play effect" of the inerter (see e.g., [18]). The latter gap element is connected in series with a viscoelastic element, following the work Papageorgiou et al. [19], with stiffness k_s and damping c_s. Ultimately, three different internal rotational DOFs, θ_P, θ_S, and θ_G, shown in Figure 4(b) are used to define the torques developed in the inerter mechanical model given as

$$T_P = k_S(\theta_S - \theta_P) + c_S\left(\dot{\theta}_S - \dot{\theta}_P\right) \text{ and } T_G = J_B\ddot{\theta}_G + c_B\dot{\theta}_G, \tag{2}$$

where $\theta_P = u_T/r_P$. The nonlinear force-deformation relationship characterizing the behaviour of the prototype non-ideal inerter device is written as [16]

$$\mathrm{F_B} = \mathrm{f_y sign}(\dot{\mathrm{u}}_\mathrm{T}) + \mathrm{T_P}/\mathrm{r_P} \tag{3}$$

where

$$\begin{cases} T_P = T_G \leq 0 & \text{for} \quad \theta_G - \theta_S = -\varepsilon_1 \\ T_P = T_G = 0 & \text{for} \quad -\varepsilon_1 < \theta_G - \theta_S < \varepsilon_2 \\ T_P = T_G \geq 0 & \text{for} \quad \theta_G - \theta_S = \varepsilon_2 \end{cases} \tag{4}$$

Having defined analytically force-deformation relationships for the HDRIs and the inerter device, equations of motion of the nonlinear 2-DOF numerical model in Figure 4 are written as

$$\begin{aligned} m_I \ddot{u}_I + F_I &= -m_I \ddot{u}_G + F_T \\ m_T \ddot{u}_T &= -m_T \ddot{u}_G - F_B - F_T \end{aligned} \tag{5}$$

where $F_I = F_{EI} + F_{DI}$ and $F_T = F_{ET} + F_{DT}$.

A standard least-squares optimization problem is formulated and numerically solved to determine the total of 8 coefficients involved in the definition of the two HDRIs of the physical model by minimizing the sum of the squared differences between experimentally and numerically obtained FRFs in terms of PS deflection and acceleration, secondary mass deflection, and inerter force. Results are as follows: $k_{1I} = 5.00 \times 10^4\ N/m$, $k_{2I} = 1.52 \times 10^6\ N/m^2$, $k_{3I} = 1.90 \times 10^4\ N/m^3$, $c_I = 538.13\ Ns/m$, $k_{1T} = 6.03 \times 10^4\ N/m$, $k_{2T} = 3.87 \times 10^5\ N/m^2$, $k_{3T} = 1.94 \times 10^6\ N/m^3$ and $c_T = 409.15\ Ns/m$. In determining the above values, the 8 parameters involved in the nonlinear force-deformation relationship of the inerter prototype were taken as: $f_y = 7.3\ N$, $r_P = 0.018\ m$, $J_B = 1.55 \times 10^{-2}\ kgm^2$, $k_S = 187.16\ Nm/rad$, $c_S = 0.85\ Nms/rad$, $\varepsilon_1 = 0.0084\ rad$, $\varepsilon_2 = 0.0056\ rad$ and $c_B = 0.03\ Nms/rad$, based on experimental component testing data detailed in [16].

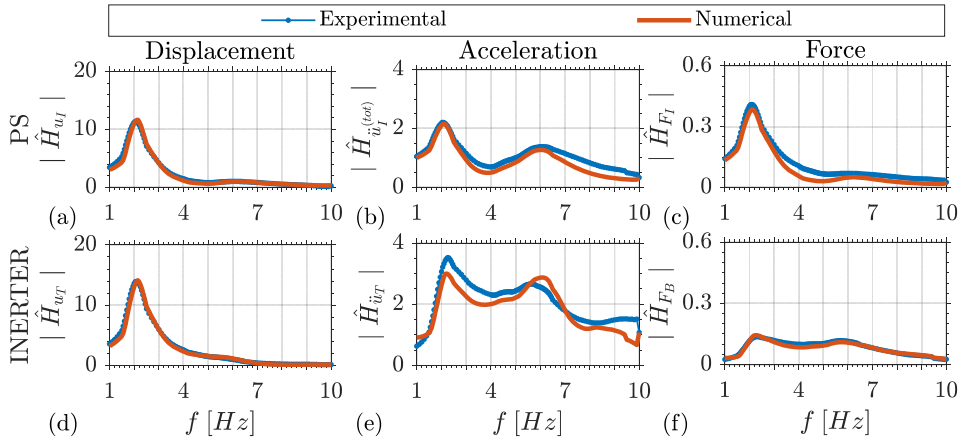

Figure 5: Comparison of experimental and numerical normalized FRFs of TMDI controlled PS with inertance ratio $\beta = 0.383$ under sine-sweep excitation with $PGA = 0.10g$.

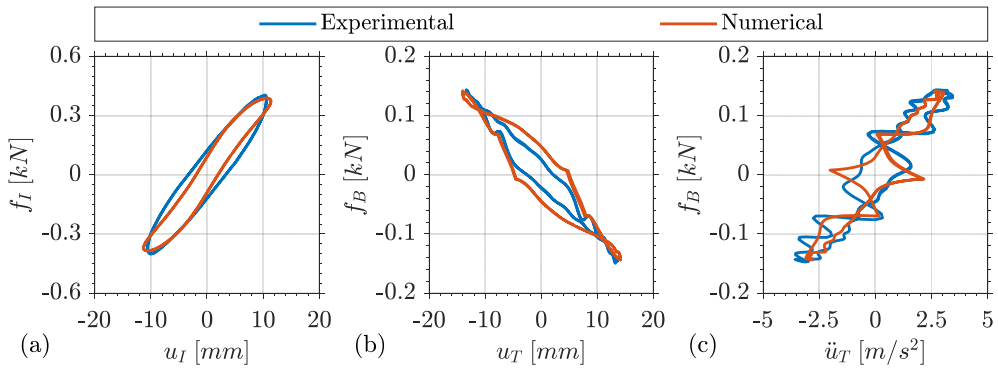

Figure 6: Comparison of experimental and numerical force-deformation curves for of TMDI controlled PS with inertance ratio $\beta = 0.383$ under sine-sweep excitation with $PGA = 0.10g$ and at resonant frequency 2.25 Hz.

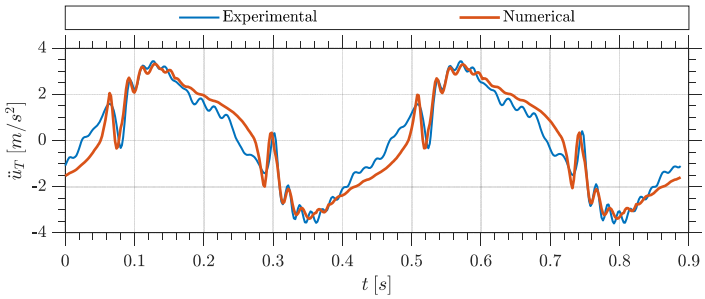

Figure 7: Comparison of experimental and numerical time history of acceleration of inerter for TMDI controlled PS ($\beta = 0.383$) under sine-sweep excitation with $PGA = 0.10g$ and at resonant frequency 2.25 Hz.

Figures 5-7 compare various experimental and numerically derived FRFs, force-deformation relationships, and response time-histories. Evidently, the developed 2DOF nonlinear dynamic model captures well the experimental data and can faithfully represent the response of both the PS and the TMDI control system. This verification gives confidence to the quality and validity of the experimental data presented in Section 3 and their interpretation.

5 CONCLUSIONS

Preliminary results from a novel shake table testing campaign were presented involving a physical specimen of TMDI-equipped SDOF structure with a custom-built rack-and-pinion flywheel-based grounded inerter exhibiting nonlinear structural behavior under harmonic excitation with varying frequency. Further, a 2DOF nonlinear numerical model of the test specimen was considered accounting for non-ideal inerter device behavior and for nonlinear elastic response of the specimen and was successfully fitted to experimental data through the solution of a least-squares optimization problem. Experimental parametric analyses for different excitation amplitude and inertance property confirmed results from previous theoretical studies, assuming linear structural response and ideal inerter behaviour, for the herein studied inerter-equipped system. That is, the system becomes more flexible (resonant frequencies reduce) and the TMDI becomes more effective in suppressing primary structure motion as nominal inertance increases despite deviations from the ideal inerter behavior. Moreover, the fact that the nonlinear numerical model, which considers well-established in the literature force-deformation relationships for the isolators and for the inerter, was able to capture satisfactorily experimental response data appraises positively the validity of the undertaken experimental campaign and the rationality of the obtained experimental results. Further experimental shake table testing data, not included herein due to space limitation, will be disseminated in future publications by the authors.

REFERENCES

[1] K. Ikago, K. Saito, N. Inoue, Seismic control of single-degree-of-freedom structure using tuned viscous mass damper. *Earthquake Engineering and Structural Dynamics*, **41**, 453-474, 2012.

[2] I.F. Lazar, S.A. Neild, D.J. Wagg, Using an inerter-based device for structural vibration suppression. *Earthquake Engineering and Structural Dynamics*, **43**(8), 1129–1147, 2012.

[3] L. Marian, A. Giaralis, Optimal design of a novel tuned mass-damper-inerter (TMDI) passive vibration control configuration for stochastically support-excited structural systems. *Probabilistic Engineering Mechanics*, **38**, 56–164, 2014.

[4] D. Pietrosanti, M. De Angelis, M. Basili, Optimal design and performance evaluation of systems with Tuned Mass Damper Inerter (TMDI). *Earthquake Engineering and Structural Dynamics*, **46**(8), 1367–1388, 2017. https://doi.org/10.1002/eqe.2861.

[5] M.C. Smith, Synthesis of mechanical networks: the inerter. *IEEE Transactions on Automatic Control*, **47**(10), 1648–1662, 2002.

[6] A. Giaralis, A.A. Taflanidis, Optimal tuned mass-damper-inerter (TMDI) design for seismically excited MDOF structures with model uncertainties based on reliability criteria. *Structural Control and Health Monitoring*, **25**, e2082, 2018.

[7] A.A. Taflanidis, A. Giaralis, D. Patsialis, Multi-objective optimal design of inerter-based vibration absorbers for earthquake protection of multi-storey building structures. *Journal of the Franklin Institute*, 2019. DOI: 10.1016/j.jfranklin.2019.02.022.

[8] D. De Domenico, G. Ricciardi, An enhanced base isolation system equipped with optimal tuned mass damper inerter. *Earthquake Engineering & Struct. Dyn.*, 47, 1169-1192, 2018.

[9] M. De Angelis, A. Giaralis, F. Petrini, D. Pietrosanti, Optimal tuning and assessment of inertial dampers with grounded inerter for vibration control of seismically excited base-isolated systems. *Engineering Structures*, **196**, 109250, 2019.

[10] M. Basili, M. De Angelis, D. Pietrosanti, Modal analysis and dynamic response of a two adjacent single degree of freedom systems linked by spring-dashpot-inerter elements. *Engineering Structures*, **174**, 736-752, 2018.

[11] M. Basili, M. De Angelis, D. Pietrosanti, Defective two adjacent single degree of freedom systems linked by spring-dashpot-inerter for vibration control. *Engineering Structures*, **188**, 480-492, 2019. https://doi.org/10.1016/j.engstruct.2019.03.030.

[12] P. Brzeski, P. Perlikowski, Effects of play and inerter nonlinearities on the performance of tuned mass damper. *Nonlinear Dynamics*, **88**, 1027–1041, 2017.

[13] D. De Domenico, P. Deastra, G. Ricciard, N.D. Sims and D.J. Wagg, Novel fluid inerter based tuned mass dampers for optimised structural control of base-isolated buildings. *Journal of the Franklin Institute*, 2018. DOI: 10.1016/j.jfranklin.2018.11.012

[14] A. Gonzalez-Buelga, I.F. Lazar, J.Z. Jiang, S.A. Neild, D.J Inman, Assessing the effect of nonlinearities on the performance of a tuned inerter damper. *Structural Control and Health Monitoring*, **24**(3), e1879, 2017.

[15] P. Brzeski, M. Lazarek, P. Perlikowski, Experimental study of the novel tuned mass damper with inerter which enables changes of inertance. *Journal of Sound and Vibration*, **404**, 47–57, 2017.

[16] D. Pietrosanti, Studio dell'Inerter come dispositivo innovativo nel controllo delle vibrazioni (Study of Inerter as innovative device in vibration control). *Ph.D. Thesis, Sapienza University of Rome*, 2019.

[17] A.A. Markou, G.D. Manolis, Mechanical models for shear behavior in high damping rubber bearings. *Soil Dynamics and Earhtquake Engineering*, **90**, 221-226, 2016.

[18] F. Scheibe, M.C. Smith, A behavioral approach to play in mechanical networks. *SIAM Journal of Control Optimization*, **47**(6), 2967–2990, 2009.

[19] C. Papageorgiou, N.E. Houghton, M.C. Smith, Experimental testing and analysis of inerter devices. *Journal of Dynamic Systems, Meas. and Control*, **131**, 011001, 2008.